Preliminary Analysis of Particulate Infiltration into Space System Volumes

30 September 2007

Prepared by

De-Ling Liu and Kenneth T. Luey
Space Materials Laboratory
Laboratory Operations

Prepared for

SPACE AND MISSILE SYSTEMS CENTER
AIR FORCE SPACE COMMAND
483 N. Aviation Blvd.
El Segundo, CA 90245-2808

20071108158

Engineering and Technology Group

**THE AEROSPACE
CORPORATION**
El Segundo, California

Michael Zambrana
SMC/EA

REPORT DOCUMENTATION PAGE

Public reporting burden for this collection of information is estimated to average 1 hour per response, including the time for reviewing instructions, searching existing data sources, gathering and maintaining the data needed, and completing and reviewing this collection of information. Send comments regarding this burden estimate or any other aspect of this collection of information, including suggestions for reducing this burden to Department of Defense, Washington Headquarters Services, Directorate for Information Operations and Reports (0704-0188), 1215 Jefferson Davis Highway, Suite 1204, Arlington, VA 22202-4302. Respondents should be aware that notwithstanding any other provision of law, no person shall be subject to any penalty for failing to comply with a collection of information if it does not display a currently valid OMB control number. **PLEASE DO NOT RETURN YOUR FORM TO THE ABOVE ADDRESS.**

1. REPORT DATE (DD-MM-YYYY)	2. REPORT TYPE	3. DATES COVERED (From - To)
30-09-2007		

4. TITLE AND SUBTITLE

Preliminary Analysis of Particulate Infiltration into Space System Volumes

5a. CONTRACT NUMBER
FA8802-04-C-0001

5b. GRANT NUMBER

5c. PROGRAM ELEMENT NUMBER

6. AUTHOR(S)

De-Ling Liu and Kenneth T. Luey

5d. PROJECT NUMBER

5e. TASK NUMBER

5f. WORK UNIT NUMBER

7. PERFORMING ORGANIZATION NAME(S) AND ADDRESS(ES)

The Aerospace Corporation
Laboratory Operations
El Segundo, CA 90245-4691

8. PERFORMING ORGANIZATION REPORT NUMBER

TR-2007(8565)-7

9. SPONSORING / MONITORING AGENCY NAME(S) AND ADDRESS(ES)
Space and Missile Systems Center
Air Force Space Command
483 N. Aviation Blvd.
El Segundo, CA 90245

10. SPONSOR/MONITOR'S ACRONYM(S)
SMC

11. SPONSOR/MONITOR'S REPORT NUMBER(S)

12. DISTRIBUTION/AVAILABILITY STATEMENT

Approved for public release; distribution unlimited.

13. SUPPLEMENTARY NOTES

14. ABSTRACT

To understand the dynamics of airborne particulate intrusion into a simulated space telescope and other space system volumes, a simple model was developed to predict the extent to which ambient particles penetrate through vent holes and enter the volume interiors after the purge is off. This report describes the mathematical modeling analysis, experimental data from laboratory studies, and field measurements from launch processing. It was found that the characteristic time for infiltrating particulates to reach a saturation level inside the volume can be characterized by the air exchange rate and particle deposition rate. After the purge is turned off, the steady-state particulate concentrations inside the volume are governed by the ambient, air cleanliness level outside the telescope, air exchange rate, and particle deposition rate.

15. SUBJECT TERMS

Particulate contamination, Telescope infiltration, Intrusion

16. SECURITY CLASSIFICATION OF:

a. REPORT	b. ABSTRACT	c. THIS PAGE
UNCLASSIFIED	UNCLASSIFIED	UNCLASSIFIED

17. LIMITATION OF ABSTRACT

18. NUMBER OF PAGES

19

19a. NAME OF RESPONSIBLE PERSON
De-Ling Liu

19b. TELEPHONE NUMBER (include area code)
(310)336-0062

Standard Form 298 (Rev. 8-98)
Prescribed by ANSI Std. 239.18

Acknowledgments

Contents

Figures

Tables

1. Introduction

Purging is a common scheme to protect sensitive surfaces of payloads and spacecraft during testing, integration, and launch vehicle encapsulation. It provides particle-free gas (typically nitrogen) into the enclosed volume, preventing particle fallout onto contamination-sensitive surfaces by establishing positive pressure. However, the purge is often turned off, either by processing plan, or by inadvertent action. In the aerospace contamination control community, correlations developed by Buch and Barsh (1987) and Hamberg (1982) are used to perform payload purge outage analysis in order to establish appropriate purge outage requirements. In reality, the transport of particles can be predicted by parameters that characterize air-exchange rate and particle loss rate inside the space system volumes. In this report, a physical model is presented to provide the dynamic picture of particle intrusion into an enclosed volume once the purge is turned off. Preliminary data of laboratory measurements from a simulated space telescope were obtained to compare with the model analysis. In addition, particle monitoring results inside the payload fairing (PLF) during down hoist on launch pads provide supporting evidence of particle infiltration data.

2. Method

2.1   Modeling Analysis

Assume an enclosed volume, such as a space telescope (ST), is purged to positive pressure by a gaseous nitrogen (GN_2) flow. A space vehicle enclosed in a purged payload fairing can also be assumed. When the purge is on, the particulate level inside the volume is usually very low. When the purge is turned off, the ambient airborne particles are transported into the volume owing to random thermal motions of air molecules or natural convection in the presence of a temperature gradient. Particles infiltrate through the designed vent holes and unintentional leakage paths. Inside the volume, the particle concentration change as a function of time can be represented by the following equation:

$$\frac{dC_{in}}{dt} = p\lambda C_{out} - (\lambda + k)C_{in}, \qquad (1)$$

where C_{in} and C_{out} are the particle number concentration inside and outside the control volume (CV; mass/cm^3 or #/cm^3), respectively; p is the particle penetration factor (dimensionless) through the leaks of CV; λ and k are the air-exchange rate (Volume Air Changes per Hour, ACH, h^{-1}) and particle deposition rate (h^{-1}) onto interior surfaces of the CV, respectively. The schematic representation of the mathematical model is illustrated Figure 1. A detailed configuration of the payload is not required for the current modeling analysis; here, a cylindrically shaped enclosure is used to represent a space telescope.
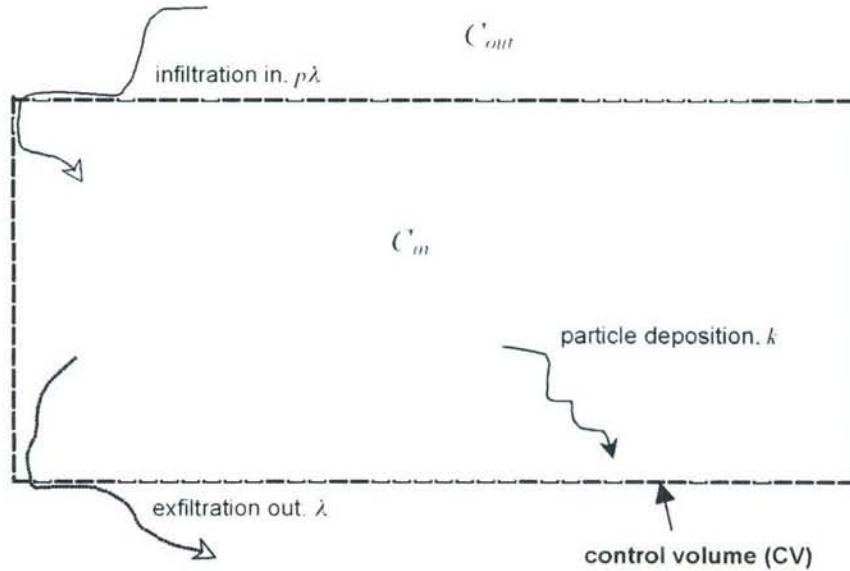

Figure 1.   Schematic representation of the air exchange (infiltration and exfiltration), as well as particle deposition loss components in the mechanistic model.

Equation (1) is the mass balance equation, which simply states that the rate of particle concentration change is governed by a *source* term, $p\lambda C_{out}$, and a *sink* term, $(\lambda+k)C_{in}$. In the schematic shown in Figure 1, the *source* term is the infiltration of particles from the exterior ambient environment into the CV by making perhaps one or more right-angle turns into the CV at an air exchange rate of λ. The *sink* term refers to the processes in which airborne particles inside CV, C_{in}, are removed by means of exfiltration, λC_{in}, and deposition loss, kC_{in}. Exfiltration is the particle removal mechanism in which airborne particles are swept out of the CV by air exchange, and deposition loss is the mechanism in which airborne particles deposit onto interior surfaces of CV by gravity or diffusion. Exfiltration and deposition loss, which are two independent processes, occur at the same time. In addition, both mechanisms are well approximated as a first-order process (Nazaroff, 1989); thus, λ and k are proportional to C_{in}.

The following several paragraphs elaborate the important parameters involved:

2.1.1   Particle Deposition Loss, k

Note that particle size plays a major role in every aspect of aerosol behavior, such as the rate of deposition onto surfaces. Therefore, it is necessary in Eq. (1) to take particle size into account. This was treated by segregating particles into various size bins. Lai (2003) compiled a review of particle deposition rate, k, as a function of particle size under various settings, including the ratio of surface area to volume and airflow turbulence intensity. The distinct feature of particle deposition behaviors is that particles of 0.1–2 μm in aerodynamic diameters have the lowest deposition rates in comparison to particles smaller and larger than this size range. This means that particles of 0.1–2 μm tend to linger in air and remain airborne longer than particles <0.1 μm and >2 μm. Particles smaller than 0.1 μm are more easily removed by Brownian and turbulent diffusion, and particles larger than 2 μm are more effectively removed by gravitational settling.

2.1.2   Air Exchange, λ

Air displacement out of the control volume plays a role in removing particles, and this removal process is characterized by air-exchange rate. Air-exchange rates can be calculated as the ratio of air flowrate into (or out) of the space versus the enclosure volume under isothermal conditions in which the air volume does not expand or contract. When the CV geometry is not well defined and/or the air flowrate is hard to measure, the air-exchange rate can be determined using tracer gas techniques (see details in 2.2.2). In this manner, the air-exchange rate arises as an aggregate term to characterize the overall rate of air replenishment through all leaks and openings on the surfaces of a control volume; therefore, detailed information on the geometry of the leakage paths is not required. Air-exchange rate usually can be used to evaluate the effectiveness of airborne contaminant removal by means of the ventilation process. Particle removal by air exchange occurs at a rate independent of particle size.

2.1.3   Penetration Factor, p

The penetration factor, p, is the fraction of particles that are transported by the infiltrating air and remain airborne as air enters the control volume. The value of p may vary depending on the residence time within the leakage path, which is governed by leak dimensions and pressure differential across the openings. As expected, p is a function of particle size, and its values can be calculated for well-

4

defined, simplified leakage geometries (Liu and Nazaroff, 2001). For complicated leakage geometries, the value of p can only be determined by experiments (Liu, 2002). For particles with aerodynamic diameter smaller than 10 μm, particle penetration is expected to be complete (i.e., $p = 1$) when the air velocity within the leaks is low. Depending on the pressure differential and leakage geometry, particles larger than 10 μm are more likely to settle onto the surfaces by gravity along the leakage path ($p < 1$).

2.1.4 Solution to the Mass Balance Equation

Assuming C_{out}, λ, and k are constant over time, the time-dependent particle concentration inside the control volume, $C_{in(t)}$, can be expressed as the analytical solution to Eq. (1):

$$C_{in}(t) = \frac{p\lambda}{\lambda + k} C_{out}\left[1 - \exp\left(-(\lambda + k)t\right)\right]. \tag{2}$$

Under the circumstances in which C_{out}, λ, and k vary with time, a numerical multi-step approach for the transient mass-balance analysis can be performed to solve $C_{in(t)}$. This report omits such complexities in order to focus on the physical implications of the particle transport processes. The interpretation of Eq. (2) will be elaborated in the Results section along with experimental data.

In summary, a mechanistic view of airborne particle transport into space system volumes through infiltration, and their fate—deposition loss onto surfaces and exfiltration with outgoing air—can be represented by a material balance equation. From the perspective of contamination control, particle deposition onto surfaces is the undesirable outcome and should be minimized as possible. Based on the understanding of the particle transport processes, as well as the nature of air infiltration into space system volumes, a mathematical model can be applied to seek the important parameters that affect the extent of particle intrusion and their fallout.

2.2 Experimental

2.2.1 Experimental Setup

A simulated space telescope (SST) was designed and constructed using acrylic materials. The schematic is illustrated in Figure 2. The front cover (to the left) is designed such that maximum leakage
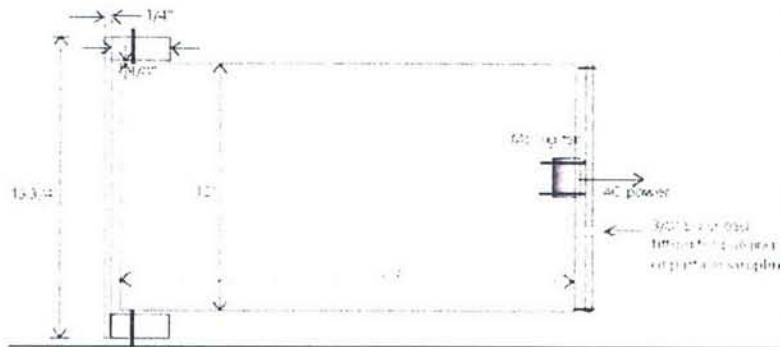

Figure 2. Side view of the mockup telescope apparatus schematic.

clearance of 1/8 in. ("most open") can be achieved, yet complete closure can also be accomplished by pushing the cover all the way to the end ("most closed"). A fan was installed to promote air mixing to meet the need of experiments when necessary.

2.2.2   Air-Exchange Rate Measurements

The rate of air displacement within the SST can be characterized in terms of air-exchange rate. A tracer gas technique was employed to determine the air-exchange rate. The concept of a tracer gas technique is to generate a uniform concentration throughout the control volume by a pulse addition of tracer gas. Once the tracer gas source has exhausted, the concentration is diluted over time owing to the replenishment of air from the exterior ambient environment that contains no tracer gas. The rate of tracer gas concentration change can be described by

$$\frac{dC}{dt} = -\lambda C, \tag{3}$$

where C is the tracer gas concentration, and λ is the air-exchange rate. After rearrangement, Eq. (2) becomes

$$\ln C_{(t)} - \ln C_{(0)} = -\lambda t, \tag{4}$$

where $C_{(0)}$ and $C_{(t)}$ are the tracer gas concentration inside SST at times 0 and t, respectively. When the air is well-mixed, plotting $\ln C$ as a function of time gives rise to a linear plot with the slope giving the air-exchange rate λ.

With respect to the selection of a tracer gas, SF_6 is an ideal candidate due to its extremely rare presence in the atmosphere, but its detection requires GC/ECD (gas chromatography equipped with electron capture detector, down to ppt level), or nondispersive IR absorption (at ppm level). Neither was available during the time frame of our experiments. Instead, CO_2 was used as the alternative for the approximately constant concentration in the ambient environment. Furthermore, CO_2 monitors are readily available at economical costs.

Two CO_2 monitors (Telaire 7001, Engelhard) were placed inside the SST to simultaneously measure CO_2 concentrations with time. The purpose of having two monitors was to evaluate whether the air-exchange rates are different locally in the absence of mechanical mixing. To generate a pulse of CO_2 inside the tube, a small chunk of dry ice was placed into a Petri dish filled with water and placed in the center of the SST. After the fan was turned on briefly for 5–10 s to mix the air and CO_2, the dry ice along with the Petri dish were quickly removed from the SST, and the fan was turned off immediately to stop the mixing. In the experiments, two options of front-cover layout were selected: 1/8 in. clearance around the tube opening (most open), and complete closure (most closed). These two configurations were chosen to evaluate the upper and lower bounds of air-exchange rates associated with the SST configuration.

2.2.3   Particle Measurements

As mentioned earlier, purging is a common scheme to protect sensitive surfaces from contamination inside space system volumes. Therefore, it is important to predict how long it takes for ambient particulates to infiltrate into a space system volume when the purge is taken away either on purpose or unintentionally.

A set of simple experiments was carried out to test this. The SST is purged with filtered, particle-free air (HEPA capsule, Pall Life Sciences) until the measured particle concentrations inside the SST were reduced to a negligible level. With the front cover oriented in the designated fashion (most open or most closed), the purged air was stopped, and the ambient air was allowed to bring in the particles from outside the SST. The particle concentration inside the SST was determined using a handheld particle counter (ARTI HHPC-6, HACH Ultra Analytics) operated at 0.1 cfm (~2.8 lpm). The detection of particles is based on light scattering principles, and the readout categorizes the particles into the following size bins: 0.3–0.5 μm, 0.5–0.7 μm, 0.7–1 μm, 1–2 μm, and 2–5 μm.

The sequence of experimental runs generally involved the following steps: (1) purge; (2) after the particles reached a negligible level, stop purge, and wait for a certain time interval; (3) take particle measurements from the sampling port. Steps (1) through (3) are repeated with the waiting time durations varied for each iteration.

The experimental setup is shown in Figure 3, and the results are presented in next section.
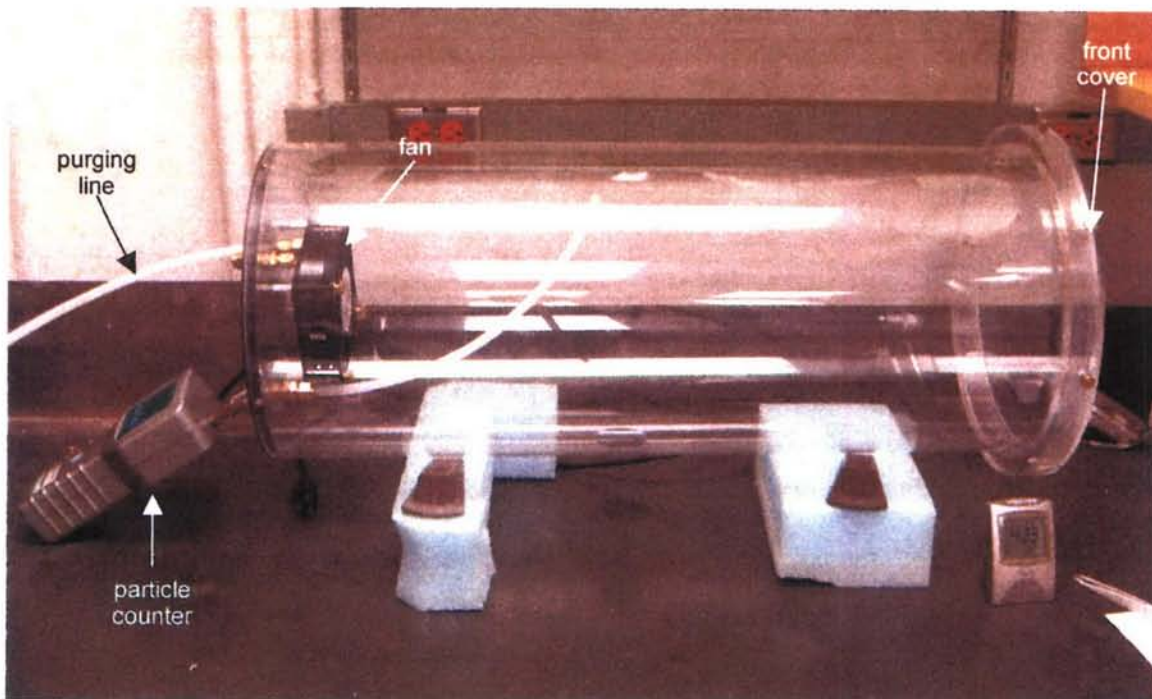

Figure 3.   Experimental setup of the particle infiltration experiments. The particle counter, connected to the SST, is shown on the left. The front cover on the right, which touches the SST opening, is at the most-closed configuration.

3. Results and Discussion

3.1 Measurements of Air-exchange Rate

Air-exchange rates of the SST were evaluated under two different settings: an unoccupied office and a clean room. They were used to represent different air turbulence intensities in the surrounding environments. The front cover was set at two closure conditions: "most closed" when the cover touches the STT, and "most open" when the minimum opening is at ~ 1/8 in. clearance.

The experimental procedures were outlined in the previous sections. Figure 4 shows a typical CO_2 concentration decay as a function of time, and a linear regression was performed to calculate the slope, which yielded the air-exchange rate. Note that when CO_2 is used as a tracer gas for air-exchange rate calculations, the background ambient concentration was subtracted from the measured values prior to evaluating the decay rate. Good air mixing inside the SST was indicated by the linear relationship of the logarithmic values of CO_2 concentration versus time.

The measured air-exchange rates are summarized in Table 1. Experiments A–D and E–G were performed in an unoccupied office and a clean room, respectively.
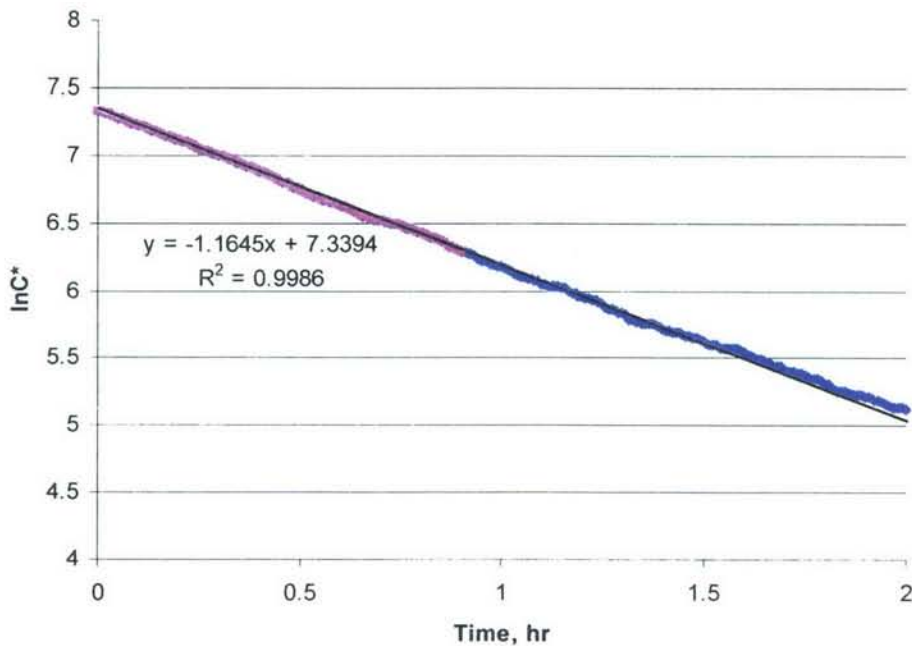

Figure 4. Air-exchange rate measured by concentration decay of CO_2 in an unoccupied office with the door closed (experiment C in Table 1). The concentration C^* is background corrected as $C^* = |CO_{2(t)} - CO_{2,b}|$.

9

Table 1. Summary of Air-Exchange Rates (ACH) Inside the SST Measured by the CO_2 Tracer Gas Technique Under Various Settings. The front cover was usually left at most-open configuration (~1/8 in. clearance) unless specified.

ACH, h^{-1}	A	B	C	D[v·]	E	F	G[v]
#1	1.9	1.3	1.2	0.1	2.7	2.8	0.2
#2	2	1.6	1.2		2.7		

Notes:

#1, #2: two CO_2 monitors placed at two different locations (left and right) inside the SST

A: with office door open and occasional people's movement

B: with office door closed (most of the time; somebody came in and stayed for 40 min, but it did not seem to influence the result)

C: with office door closed and run overnight

D: with office door closed and front cover most closed

E: in clean room

F: in clean room and use one monitor only

G: in clean room, using one monitor and with front cover most closed

[v] "most closed" configurations

[·] #2 data logger not activated

The following conclusions are drawn from the ACH measurements:

1. The differences of ACH measured at the left- and right-hand locations within the SST were insignificant, which means that the two sampling locations were subject to nearly identical air-exchange rate. Therefore, only one monitor was used in the final two experiments (F and G).

2. In the unoccupied office setting, the air was usually calm and not drafty. On the other hand, the airflow in the clean room was evidently more turbulent. When the opening leakage area was left the same, the measured ACH in the clean room was roughly twice that in the unoccupied office, as shown in the paired experiments C vs. E and D vs. G. In other words, air flow turbulence intensity in the adjacent environment plays a role in determining how fast the ambient air infiltrates into the SST.

3. Under the same settings (either unoccupied office or clean room), it is clearly seen that the measured upper bound ACHs (most open) was one order of magnitude greater than the lower bound counterparts (most closed), as indicated in the paired experiments C vs. D and E vs. G. This difference in ACHs was attributed to the available leakage area allowed for air infiltration. Therefore, air exchange between the enclosure and the surroundings can be minimized by making leakage areas as small as possible.

3.2   Particle Measurements

By particle counter measurements, particle concentration in the SST reached a negligibly low level after purging for a period of time, usually 20–30 min. The purge was stopped, and air exchange inside the SST commenced. Note that the fan was never operating during the entire particle experiment, including purging. The particle concentration inside the SST, C_{in}, was sampled again after a certain interval, e.g., 4 hours. The ambient particle concentrations, C_{out}, were also recorded immediately after C_{in} measurements. The same sequence was repeated, except varying the waiting duration,

with the aim to examine the extent to which particles infiltrate into the SST with time. The front cover was left at the "most-open" configuration (1/8 in. clearance) in this experiment.

Figure 5 represents the measured particle concentration ratio (C_{in}/C_{out}) over time for particles of 0.3–0.5 µm, as indicated by diamonds. Particles in this size range were chosen because (1) they are one of the size bins from the particle counter readout; (2) they have the strongest tendency to remain air-borne since they are most difficult to be removed either by diffusion or gravity. As a result, one would expect that 0.3–0.5 µm particles exhibit transport properties most similar to air molecules. In addition, this particle size range has the greatest particle population in ambient air (due to the least tendency for deposition loss), thus offering good counting statistics. Therefore, measuring particles in this size range provides a good indication to the dynamics of particle infiltration processes.

The absolute particle concentrations measured inside the SST, C_{in}, are also plotted in Figure 5, as depicted by squares. Significant fluctuations are observed by measuring the particle concentration C_{in} alone since C_{in} is strongly influenced by the ambient particle level C_{out} that feeds into the SST. The ambient particle concentration C_{out} fluctuated significantly with time. On the contrary, the ratio of C_{in}/C_{out}, ranging from 0.59 to 0.87 as grouped in the dashed rectangular frame, appears to have the normalization effect, which, in turn, helps damping the fluctuations.

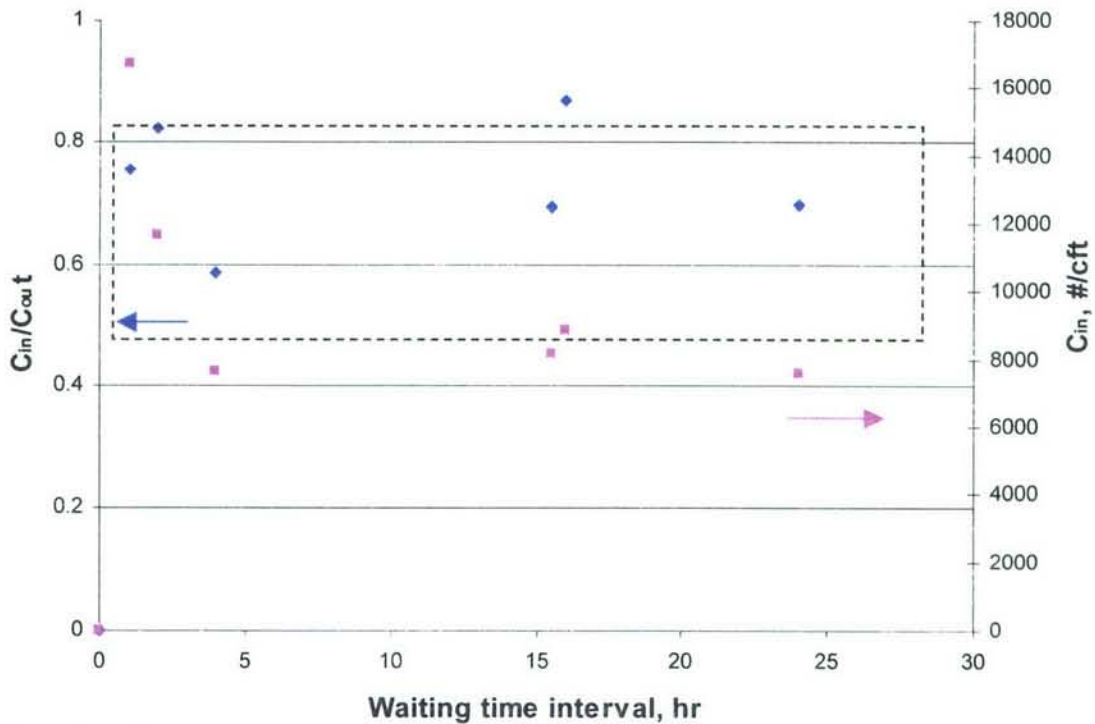Figure 5. Measured particle concentration ratio, C_{in}/C_{out} as a function of time in the purge-wait-sample procedures indicated by diamonds (♦). The data points shown in squares (■) represent the measured particle concentrations inside the SST at the designated waiting time interval. The cover was at the "most-open" configuration.

The ratios of C_{in}/C_{out} in Figure 5 demonstrate that the particle level inside the SST, C_{in}, seems to reach an equilibrium state with respect to the ambient particle concentration, C_{out}, regardless of the waiting time interval between purge/pump cycles. To take a closer look at the dynamics of particle concentration growth, a shorter waiting time interval was employed; the results are shown in Figure 6. Different from the previous protocol, the data points in Figure 6 were obtained from sampling the air inside the tube with one purge only, and the concentration rise was captured by a brief sampling of the particle counter at different sampling times. Also different from the prior experiment is that the front cover was at the "most-closed" configuration. The air-exchange rate for this setting was estimated to be ~0.1 h^{-1}.

Four iterations were conducted, and Figure 6 illustrates the rise of 0.3–0.5 μm particle concentrations as a function of time. The legends indicate the number of air samples withdrawn using the particle counter, and each sampling action lasted approximately 30 s. Note that it is not desirable to have the particle counter running continuously throughout the waiting duration because the air sampling action from the particle counter induces air movement, which, in turn, leads to artificially enhanced air exchange.

From Figure 6, it is seen that the characteristic time for particles to reach the steady-state concentration was approximately one hour, and the concentrations appeared to maintain at relatively constant level regardless of the duration of particle infiltration processes.
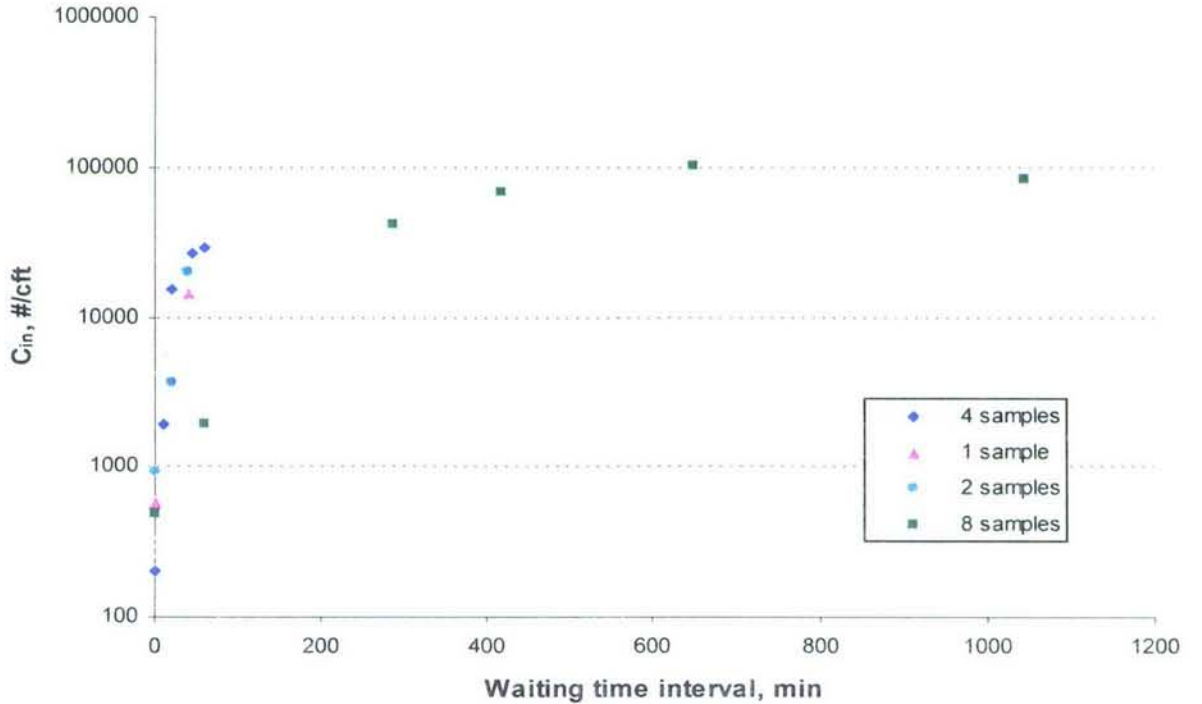

Figure 6. Particle concentration growth with time after purging has stopped. Note that only one purge was used for each iteration. The front cover of the STT is at the "most-closed" configuration.

12

3.3   Results from Modeling Analysis

As mentioned in 2.1, the dynamics of particle transport from the ambient environment into the control volume can be analyzed using a mechanistic model, as demonstrated by Eq. (1). The key parameters are air-exchange rate (ACH), λ, and particle deposition coefficient, k, where k is a function of particle size. Thus, one should expect that the extent of particle concentration rise by means of infiltration should vary according to particle sizes.

According to the mathematical expression of Eq. (2), Figure 7 illustrates the predicted particle concentration growth with time under several different postulated scenarios in which ACH λ and various particle deposition rates k were assumed. After rearrangement and assuming $p = 1$, Eq. (2) becomes

$$\frac{C_{in}(t)}{C_{out}} = \frac{\lambda}{\lambda + k}\left[1 - \exp(-(\lambda + k)t)\right]. \tag{5}$$

Five particle deposition rates ranging from 0.05 to 10 h^{-1} were used under ACHs of 0.1 and 2 h^{-1}, which, in terms of order of magnitude, represent the air exchange obtained from the prior tracer gas experiments when the cover was at "most-closed" and "most-open" configurations. Depending on the surface area-to-volume ratio (S/V),[*] 0.2–1 h^{-1} is the range of particle deposition rate for 0.3-μm particles, and 10 h^{-1} or higher is a reasonable approximation for 5-μm particles inside an enclosure such as SST (Lai, 2003). This mathematical analysis is helpful to gain insights into the relative importance of air exchange and particle deposition to the overall concentration-time profile since they are the two competing mechanisms responsible for particle loss in the SST.

From Figure 7(a), it is evident that after a certain time frame, particle concentrations grow from zero to a fixed level—a steady-state concentration. By definition, the steady-state concentration does not change with time, and the value can be estimated as

$$C_{in} = \frac{\lambda}{\lambda + k}C_{out} \tag{6}$$

when t in Eq. (5) goes to infinity. At steady state, the particles brought into the SST from exterior ambient air (λC_{out}, the *source* term) is balanced by particle loss inside the SST due to deposition onto the surfaces and air exchange that sweeps particles out (kC_{in} and λC_{in}, the *sink* terms).

Another distinct feature from the mathematical analysis as shown in Figure 7 is the curvature for the concentration rise, which can be captured by the parameter of *characteristic time* τ, given by

$$\tau \sim \frac{1}{\lambda + k}. \tag{7}$$

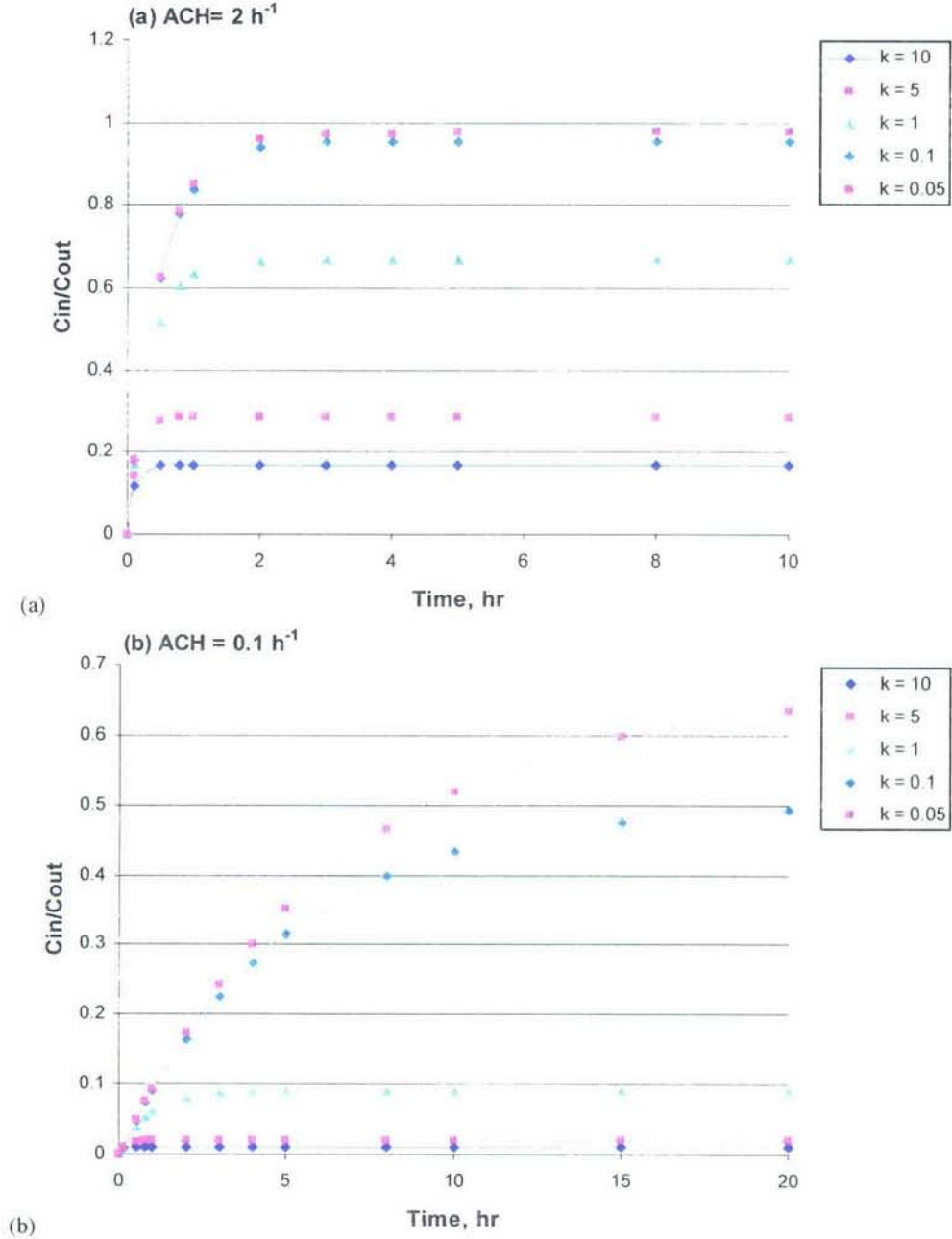[*] A normalized indicator of available surfaces for particle deposition

Figure 7. The growth of particle concentrations inside the SST as a function of time
predicted by Eq. (5), which is the analytical solution of the governing
equation describing particle infiltration into the SST. Five different parti-
cle deposition rates, k, from 0.05 to 10 h^{-1} under ACH of 2 and 0.1 h^{-1} were
considered in this modeling analysis.

τ is the time required for the system to relax from its initial condition to the steady state. Table 2
gives a summary of τ values as well as the steady-state C_{in}/C_{out} ratio associated with the above hypo-
thetical scenarios. It can be seen that given the same k, it is predicted to take less time for the system
with higher ACH to reach steady state. For instance, assuming $k = 1$ h^{-1}, the characteristic times

Table 2. The Characteristic Times and Steady-State C_{in}/C_{out} Calculated in the Postulated Particle Infiltration Scenarios Based on the Mathematical Model Analysis

| Particle Deposition | Air-exchange Rate λ, h^{-1} | | | |
| | 0.1 | | 2 | |
rate k, h^{-1}	τ	C_{in}/C_{out}	τ	C_{in}/C_{out}
0.05	6.7	0.67	0.49	0.98
0.1	5.0	0.5	0.48	0.95
1	0.9	0.09	0.33	0.67
5	0.2	0.02	0.14	0.29
10	0.1	0.01	0.08	0.17

estimated to establish steady state are 0.9 h for ACH = 0.1 h^{-1}, and ~ 0.3 h for ACH = 2 h^{-1} system, respectively. However, this discrepancy in characteristic time is not as pronounced when k becomes dominant, i.e., particle deposition becomes the important mechanism to control how fast particles are removed from the system. Furthermore, one can also see that greater values of k, as reflected by larger particles, also lead to more particle fallout, as a result, lowering the steady-state C_{in}/C_{out} ratios.

Particle deposition rate k is governed by particle size as well as the degree of airflow turbulence *inside* the control volume; higher turbulence intensity results in greater particle deposition rate owing to stronger near-surface air flow conditions (Thatcher et al., 2002, Nazaroff and Cass, 1989). Therefore, a quiescent air flow condition is expected to result in a smaller k, which is advantageous when minimized particle fallout is the goal. In addition, reducing air exchange between the control volume and the ambient environment would be a favorable approach (assuming the CV itself is clean, free of particles, and the exterior ambient environment contains particles). Lower air exchange can delay the progress that particles infiltrate into the system; albeit, for large particles this does not seem to make a significant difference.

On the contrary, higher air flow turbulence *surrounding* the SST results in faster air exchange, as suggested in the previous air-exchange rate experiments. This implies that particles that are carried by the ECS (Environmental Control System) are anticipated to infiltrate into the space system volumes rapidly, perhaps within 30 min or less if the ACH inside the volumes induced by the turbulent ECS flow is ~ 2 h^{-1} or higher. It would be critical to evaluate the range of ACH inside PLF when ECS is on in order to estimate how fast particles are transported into the payload. Once particles get in, their airborne concentration can be predicted according to the mathematical expression shown in Eq. (5), and the concentration should not exceed the surroundings (normally Class 5K or better for ECS GN2 inside PLF).

3.4 Payload Fairing Studies

This mechanistic approach can be applied to various scenarios. For example, the scale of the control volume can be extended to a Delta IV PLF to examine the transport of atmospheric particles through the air leaks. When the ECS air is on, the positive pressure caused by the ECS flow prevents the atmospheric particles from infiltration. Once the ECS purge is off, the positive pressure is no longer available. Therefore, the particle concentration inside the PLF begins to increase as a result of wind-induced infiltration, which is evidenced by particle monitoring data inside PLF during on-pad opera-

tions, as shown in Figures 8 and 9. In particular, the particle concentration growth pattern indicated in Figure 9 is consistent with our modeling analysis.
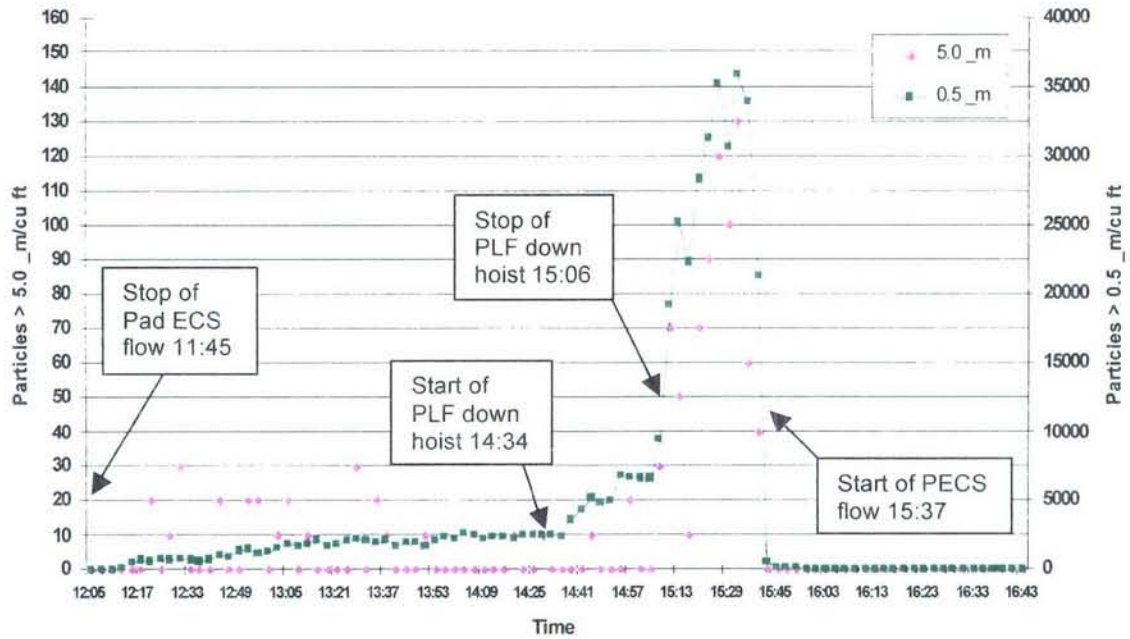

Figure 8. Particle monitoring data inside PLF during down-hoist period (provided by United Launch Alliance). The particle counts were determined by MetOne 227A Particle Counter.
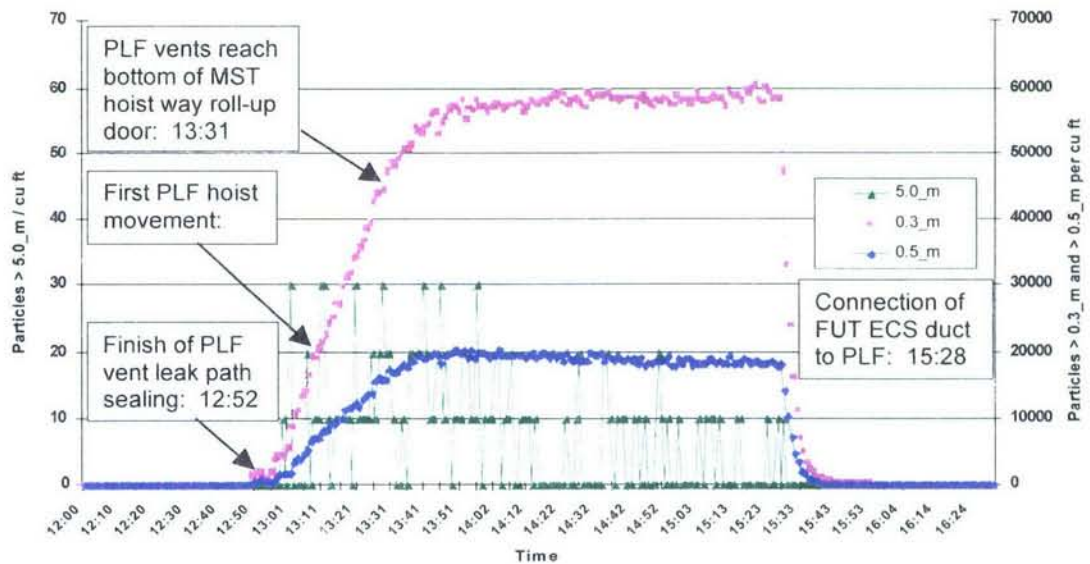

Figure 9. Particle monitoring data inside PLF during down-hoist period (provided by Boeing). The particle counts were determined by MetOne HHPC-6 Particle Counter. By the same token, the minimum purge outage during payload testing and integration can be estimated using the same analytical approach. Based on the current analysis, a more refined model that accounts for particle deposition flux (or fallout rate) will be necessary to develop and to validate in order to advance our understanding on the time-dependent relationship between air cleanliness class and surface cleanliness level, which results from accumulated buildup of airborne particle deposition.

4. Conclusions

A preliminary analysis was conducted to provide physical insights into the dynamics of airborne particle transport into a generic space system volume. A mechanistic model based on material balance was employed to account for the particle transport processes by means of air exchange and particle deposition onto interior surfaces. The analytical results show that the airborne particle concentration change inside the control volume is governed by two parameters: *air-exchange rate* (ACH), λ; and *particle deposition rate, k*. The air-exchange rate can be measured using a tracer gas technique, as demonstrated in this report, and the size-specific particle deposition rates can be determined experimentally, or approximated from the existing literature.

Some preliminary data from the laboratory experiments and particle monitoring data inside PLF during on-pad operations are provided to complement the modeling predictions. From the data, it can be seen that after the purge is off, the particle concentration increases with time until it reaches the steady state, which stays at a constant level relative to the ambient particle concentration and does not change with time. The pace of particle concentration increase can be approximated by the parameter of *characteristic time*, τ, which is associated with λ and k, as indicated in Eq. (7). The steady-state particle concentration is governed by λ, k, as well as the ambient concentration, C_{out}, as shown in Eq. (5).

This simple mathematical model is applicable in scenarios such as (1) particulate intrusion into a space telescope when purge is off; (2) particle infiltration into PLF when ECS GN_2 interruption occurs. More efforts will be needed to characterize size-specific particle deposition rate under the air flow conditions representing the actual degree of turbulence inside space system volumes while air-exchange rates are measured simultaneously. Particle fallout rates yielded from such deposition experiments are expected to help elucidate the time-dependent correlation between air cleanliness class and surface particle cleanliness level, and to further establish physical-based purge outage requirements.

References

1. Buch, J. D. and Barsh, M. K., "Analysis of particulate contamination buildup on surfaces," *SPIE proceedings: optical system contamination: effect, measurement, control* **777**: 43–54, 1987.

2. Hamberg, O., "Particle fallout predictions for cleanrooms," *Journal of Environmental Science* **25**, 15, 1982.

3. Lai, A. C. K., "Particle deposition indoors: a review," *Indoor Air* **12**, 211–214, 2002.

4. Liu, D.-L. and Nazaroff, W. W. "Modeling Pollutant Penetration Across Building Envelopes," *Atmospheric Environment* **35**, 4451–4462, 2001.

5. Liu, D.-L. and Nazaroff, W. W., "Particle Penetration through Building Cracks," *Aerosol Science and Technology* **37**, 565–573, 2003.

6. Liu, D.-L., "Air pollutant penetration through airflow leaks into buildings," Ph.D. dissertation, University of California at Berkeley, 2002.

7. Nazaroff, W. W. and Cass, G. R., "Mass-transport aspects of pollutant removal at indoor surfaces," *Environment International* **15**, 567-584, 1989.

8. Thatcher, T. L., Lai, A. C. K, Moreno-Jackson, R., Sextro, R. G., and Nazaroff, W. W., "Effects of room furnishings and air speed on particle deposition rates indoors," *Atmospheric Environment* **36**, 1811–1819, 2002.

LABORATORY OPERATIONS

The Aerospace Corporation functions as an "architect-engineer" for national security programs, specializing in advanced military space systems. The Corporation's Laboratory Operations supports the effective and timely development and operation of national security systems through scientific research and the application of advanced technology. Vital to the success of the Corporation is the technical staff's wide-ranging expertise and its ability to stay abreast of new technological developments and program support issues associated with rapidly evolving space systems. Contributing capabilities are provided by these individual organizations:

Electronics and Photonics Laboratory: Microelectronics, VLSI reliability, failure analysis, solid-state device physics, compound semiconductors, radiation effects, infrared and CCD detector devices, data storage and display technologies; lasers and electro-optics, solid-state laser design, micro-optics, optical communications, and fiber-optic sensors; atomic frequency standards, applied laser spectroscopy, laser chemistry, atmospheric propagation and beam control, LIDAR/LADAR remote sensing; solar cell and array testing and evaluation, battery electrochemistry, battery testing and evaluation.

Space Materials Laboratory: Evaluation and characterizations of new materials and processing techniques: metals, alloys, ceramics, polymers, thin films, and composites; development of advanced deposition processes; nondestructive evaluation, component failure analysis and reliability; structural mechanics, fracture mechanics, and stress corrosion; analysis and evaluation of materials at cryogenic and elevated temperatures; launch vehicle fluid mechanics, heat transfer and flight dynamics; aerothermodynamics; chemical and electric propulsion; environmental chemistry; combustion processes; space environment effects on materials, hardening and vulnerability assessment; contamination, thermal and structural control; lubrication and surface phenomena. Microelectromechanical systems (MEMS) for space applications; laser micromachining; laser-surface physical and chemical interactions; micropropulsion; micro- and nanosatellite mission analysis; intelligent microinstruments for monitoring space and launch system environments.

Space Science Applications Laboratory: Magnetospheric, auroral and cosmic-ray physics, wave-particle interactions, magnetospheric plasma waves; atmospheric and ionospheric physics, density and composition of the upper atmosphere, remote sensing using atmospheric radiation; solar physics, infrared astronomy, infrared signature analysis; infrared surveillance, imaging and remote sensing; multispectral and hyperspectral sensor development; data analysis and algorithm development; applications of multispectral and hyperspectral imagery to defense, civil space, commercial, and environmental missions; effects of solar activity, magnetic storms and nuclear explosions on the Earth's atmosphere, ionosphere and magnetosphere; effects of electromagnetic and particulate radiations on space systems; space instrumentation, design, fabrication and test; environmental chemistry, trace detection; atmospheric chemical reactions, atmospheric optics, light scattering, state-specific chemical reactions, and radiative signatures of missile plumes.